Desalination and Water Treatment
www.deswater.com

doi: 10.5004/dwt.2017.20522

71 (2017) 359–368
April

Synthesis and characterization of *N*-succinyl-*O*-carboxymethyl chitosan for Pb(II) ions adsorption

Qingping Song*, Chongxia Wang, Jiangang Gao, Yujie Ding

School of Biochemical Engineering, Anhui Polytechnic University, Wuhu 241000, China, Tel. +86-553-2871255; Fax: +86-553-2871254; emails: adsqp@163.com (Q.P. Song), wangcx@ahpu.edu.cn (C.X. Wang), gaojiangang@ahpu.edu.cn (J.G. Gao), yujieding123@163.com (Y.J. Ding)

Received 19 August 2016; Accepted 18 January 2017

ABSTRACT

A novel *N*-succinyl-*O*-carboxymethyl chitosan (NSOC) was synthesized by a simple two-step method. *O*-carboxymethyl chitosan (OCMC) was prepared first by reacting chitosan with chloroacetic acid, and then the achieved OCMC was further succinylated by succinic anhydride in aqueous solution. The resultant NSOC was characterized by Fourier transform infrared (FTIR), elemental, ^{1}H nuclear magnetic resonance (^{1}H-NMR), scanning electron microscope (SEM) and X-ray diffraction pattern (XRD) analysis. The adsorption of Pb(II) was subsequently investigated. The adsorption isotherms obeyed the Langmuir equation, and the adsorption kinetics followed a pseudo-second-order model. FTIR and X-ray photoelectron spectra results showed that the excellent adsorption performance of NSOC for lead ions was attributed to the presence of large number of carboxyl groups.

Keywords: Adsorption; Chitosan; Succinyl chitosan; Carboxylate chitosan; Adsorption mechanism

1. Introduction

Heavy metal pollution in industrial wastewater has attracted global attention because of its adverse effects on the environment and human health. For example, lead is generated from a number of industrial sources such as storage batteries, electroplating, printing circuit board and so on. Lead is also well-known to be a cumulative poison through water intake or food chains and can cause brain damage and dysfunction of the kidneys, the liver and the central nervous system in human beings [1]. Today, several methods have been developed for removing Pb(II) from wastewater including chemical precipitation, membrane process, ion-exchange method and so on [2]. Among the applicable methods, adsorption is now recognized as an effective, efficient and economic method for heavy metal removal from wastewater [3,4].

In recent years, bioadsorbents are receiving increasing attention as nontoxic, biodegradable and biocompatible materials [5,6]. As an abundant natural polymer, chitosan (CS) is a biopolymer obtained after deacetylation of chitin and has high adsorption ability for heavy metal ions, because of its excellent metal-binding capacities, low cost, biodegradability and low toxicity [7–9]. In order to further improve the adsorption ability of CS, a great number of novel CS derivatives have been prepared by introducing new functional groups on the CS backbone [10–13].

Among all of CS derivatives, carboxylate CS derivatives have been reported to enhance heavy metals adsorption capacity due to the presence of multifunctional groups such as amino, hydroxyl and carboxylic groups. Carboxylate CS derivatives in the field of adsorption include *O*-carboxymethyl chitosan (OCMC), *N*,*O*-carboxymethyl chitosan (NOCMC), *N*-carboxymethyl chitosan (NCMC) and *N*-succinyl chitosan (NSCS) [14–16]. With respect to *N*-succinyl chitosan (NSCS), it can be obtained from simple reaction between CS and succinic anhydride. Currently, there are two main methods for the preparation of NSCS. For example, Sun et al. [16] have prepared *N*-succinyl CS derivatives. They synthesized NSCS by using treated CS, succinic anhydride in dimethyl sulfoxide solvent under heterogeneous conditions and the prepared

* Corresponding author.

NSCS was a good material for metal ion sorption [17]. Xiong et al. [18] have also prepared NSCS by dissolving CS in acetic acid solution. Certain amount of succinic anhydride was then dissolved in acetone and added to the system. The mixture was reacted in a homogeneous system.

In this paper, a water-soluble *N*-succinyl-*O*-carboxymethyl chitosan (NSOC) was synthesized by a two-step method. OCMC was first prepared by treating CS with chloroacetic acid, and then the obtained OCMC was further succinylated by succinic anhydride in aqueous media at room temperature with triethylamine as acid-binding agent. There are several advantages for synthesis of NSOC. First, hydroxyl groups of OCMC were occupied by carboxylmethyl groups, and then the free amino groups acted as useful intermediate for further chemical modifications. Second, succinylation reaction of OCMC can be accomplished easily in water under homogeneous reaction due to the good water solubility of OCMC, thus avoiding the use of organic solvent. Finally, NSOC has large number of carboxylic groups, and this enables it to show high chelation ability with various metal ions. Additionally, the chemical structure and properties of NSOC was elucidated and characterized by Fourier transform infrared (FTIR), elemental, ^{1}H-NMR, SEM and XRD analysis. The adsorption behaviors of NSOC for Pb(II) ions were subsequently investigated together with the effects of pH value and adsorption time. The adsorption kinetics, isotherms and adsorption mechanisms were also discussed in details.

2. Materials and methods

2.1. Materials

CS (93% deacetylated, viscosity average molecular weight: 620,000) was obtained from Sinopharm Chemical Reagent Co., Ltd. (Shanghai, China). All other chemicals and reagents were of analytical grade and used without purification. Metal ion solutions were prepared from analytical grade metal salts $Pb(NO_3)_2$ with distilled water.

2.2. Synthesis of NSOC

The synthesis of NSOC was carried out in two steps as shown in Fig. 1. The first step was the preparation of OCMC, and the second step was the introduction of the succinyl groups into the OCMC through a chemical reaction with succinic anhydride. The OCMC was synthesized by the method put forward by Chen and Park [19]. In brief: CS (10 g), sodium hydroxide (13.5 g) and solvent (water: 20 mL; isopropanol: 80 mL) were added into a flask to swell and alkalize for 1 h. The chloroacetic acid (15 g) was dissolved in isopropanol (20 mL) and added into the mixture dropwise for 30 min and reacted for 4 h at 50°C in water bath with continuous magnetic stirring, then stopped by adding 70% ethanol. The solid was filtered and rinsed in 70%–100% ethanol to desalt and dewater, and vacuum dried.

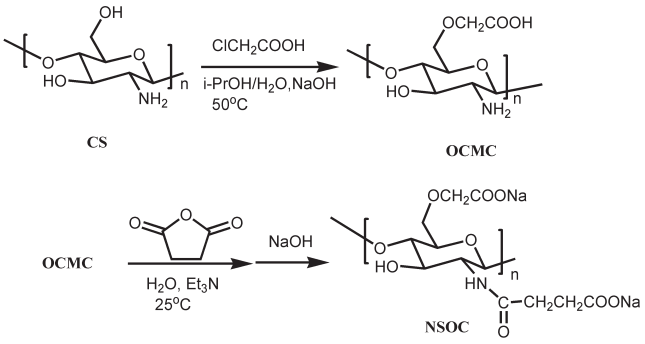

Fig. 1. Synthetic route of NSOC.

In the second step, the NSOC was obtained as follows: 2.0 g of OCMC was dissolved in H_2O (100 mL) solution for 1 h at room temperature. The succinic anhydride (2.0 g) was dissolved in acetone (10 mL) and added into the reaction mixture dropwise. After this step, 2 mL of Et_3N was added into the reaction to bind the produced acid. After a reaction of 24 h at 25°C, the solution's pH was adjusted to 8.0 by adding 5% NaOH (w/v) solution. Finally, the reaction mixture was precipitated with ethanol (300 mL), and the solid was filtered and rinsed in 80%–100% ethyl alcohol to desalt and dewater, and vacuum dried at 50°C for 12 h to achieve the final white powder product.

2.3. Adsorbent characterization

The FTIR spectra of CS derivatives were measured using a Bruker EQUINOX-55 FTIR spectrometer, and the elemental analysis was performed by using a Vario EL III analyzer (Germany) to determine the element content and the degrees of substitution in CS derivatives. ^{1}H-NMR spectra of OCMC and NSOC were recorded on a Bruker Avance-300 NMR spectrometer using D_2O as solvent. A Hitachi S-4800 (Japan) scanning electron microscope (SEM) was used to examine the microstructure of CS and NSOC. X-ray diffraction patterns of CS and NSOC were measured using an X-ray diffractometer (D8-Advance, Bruker, Germany). X-ray photoelectron spectra (XPS) of NSOC before and after Pb(II) adsorption were obtained on an ESCALAB 250 XPS spectrometer (Thermo-VG Scientific, USA).

2.4. Adsorption experiments

In adsorption experiments, a fixed amount of CS or NSOC (100 mg) and 50 mL of an aqueous solution containing Pb(II) (1,000 mg/L) were placed into a 50-mL conical flask and stirred at 200 rpm at room temperature (25°C). After stirred for a defined time, the mixture was filtered, and the final metal ion concentration of Pb(II) was measured using a Ruili WFX-110 atomic absorption spectrophotometer. Each experiment was duplicated under identical conditions. The adsorption capacity of adsorbent was calculated according to the following equation:

$$Q = \frac{V(C_0 - C_f)}{m} \quad (1)$$

where Q is the adsorption capacity (mg/g); C_0 and C_f are the initial and final concentrations of Pb(II) (mg/L), respectively; V is the volume of the Pb(II) solution (L) and m is the mass of adsorbent (g).

The effect of initial pH values on the adsorption capacity was studied by varying pH value from 2.0 to 5.5 at the

sorbent dosage of 100 mg/50 mL at 25°C for 60 min. The pH value of the solution of Pb(II) was adjusted to the required pH value by adding 0.1 mol/L HCl or 0.1 mol/L NaOH solutions, which was measured and controlled with a PHS-25 pH meter (Shanghai, China).

Adsorption kinetics allowed the equilibrium time needed to reach saturation to be determined. They were carried out at 25°C using 50 mL of metal ion solution containing the desired concentration (1,000 mg/L) and 100 mg of adsorbent, in 50 mL conical flasks. At predetermined time intervals, samples were separated, and final concentration of Pb(II) were measured. Except when pH effect was studied, all experiments were carried out at initial pH of 5.5.

Adsorption isotherms were performed at 25°C, and the stirring time was 3 h. The weight of CS or NSOC is 100 mg, and the solution volume is 50 mL with an initial metal ion concentration ranging from 500 to 1,000 mg/L.

3. Results and discussion

3.1. Characterization of adsorbent

Chemical structures and properties of the adsorbents were characterized by FTIR, elemental, ^{1}H-NMR, SEM and XRD analysis. FTIR spectra of CS and NSOC are shown in Fig. 2. The major bands for the CS can be assigned as follows: 3,431 cm^{-1} (–OH and –NH_2 stretching vibrations), 2,883 cm^{-1} (–CH stretching vibration), 1,601 cm^{-1} (–NH_2 bending vibration), 1,323 cm^{-1} (stretching vibration of C–N), 1,153 cm^{-1} (bridge-*O*-stretch), 1,036 and 1,078 cm^{-1} (primary and secondary stretching vibration of C–OH) [20,21]. In comparison with the CS spectrum, two stronger peaks at 1,577 and 1,412 cm^{-1} of NSOC were observed, which were assigned to the asymmetric and symmetric stretching of COO^- groups, respectively [22,23]. An additional peak at 1,646 cm^{-1} was assigned to –CONH–, which confirmed the formation of amide groups as a result of the reaction between succinic anhydride and amino groups of CS chains [24]. Additionally, the peak at 1,036 cm^{-1} assigned to the stretching vibration of the primary C–OH groups disappeared almost completely, indicating that the carboxymethyl reaction was accomplished via the reaction of hydroxyl groups. From these results, it was concluded that succinyl and carboxyl groups were successfully introduced into the CS backbone.

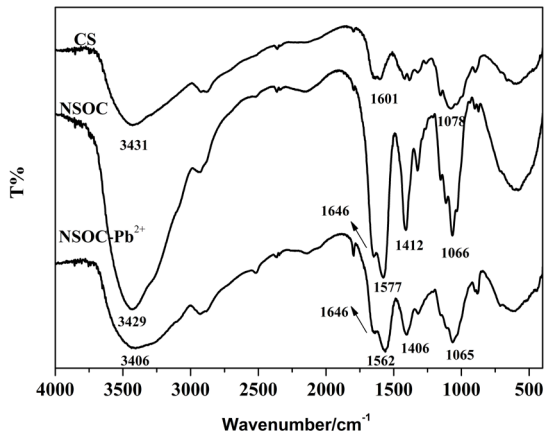

Fig. 2. FTIR spectra of chitosan (CS), and NSOC before and after adsorption of Pb(II).

Elemental analysis was also done to further characterize the composition of CS, OCMC and NSOC. The results of elemental analysis are given in Table 1. The degree of deacetylation (DD) of CS was found to be 92.6% calculated from Eq. (2). For OCMC, the degree of substitution (DS[a], defined as the number of carboxymethyl groups per hundred glucosamine units) of CS was 127.1% according to Eq. (3). In addition, the degree of succinyl substitution (DS[b]) of NSOC was 38% determined from Eq. (4).

$$\frac{C}{N} = \frac{[6 + (1 - DD) \times 2] \times 12.01}{14.01} \quad (2)$$

$$\frac{C}{N} = \frac{\{[6 + (1 - DD) \times 2] + DS^a \times 2\} \times 12.01}{14.01} \quad (3)$$

$$\frac{C}{N} = \frac{\{[6 + (1 - DD) \times 2] + DS^a \times 2 + DS^b \times 4\} \times 12.01}{14.01} \quad (4)$$

Chemical structures of OCMC and NSOC were determined by ^{1}H-NMR spectroscopy. The proton assignments of OCMC (Fig. 3) are as follows: 2.07 ppm (–COCH_3), 2.57 ppm (H2), 2.74 ppm (H2′, carbon 2 of glucosamine ring with the substituted amino group), 3.40–3.77 ppm (H3-H6), 4.00 ppm (H7, –CH_2COOD) and 4.55 ppm (H1) [25,26]. In comparison with the OCMC spectrum, the ^{1}H resonances of NSOC are as follows: 2.06 ppm (–COCH_3), 3.54–3.78 ppm (H2-H6) and 4.58 ppm (H1). In particular, the new signals of H8 (–CH_2CH_2COOD) could be found at 2.46 ppm, which confirmed that succinylation occurred on the backbone of OCMC [27,28]. Moreover, the chemical shift of the H2 signal in NSOC spectrum revealed the successful succinylation substituted on amino groups, which was in good agreement with the FTIR results. According to the area ratio of the integral peak of H8 of NSOC and H2 in CS structure, it could be known that the DS of NSOC was 40% and was good consistent with that of elemental analysis result. This result indicated that about 40% "H" in amino groups had been substituted by succinyl groups.

Table 1
Elemental analysis data for chitosan, OCMC and NSOC

Sample	C, %	N, %	C/N	DD, %	DS[a], %	DS[b], %	DS[c], %
Chitosan	41.96	7.96	5.27	92.6			
OCMC	38.01	5.10	7.45		127.1		
NSOC	36.49	4.17	8.75			38	40

[a]The degree of substitution of carboxymethyl group of CS by elemental analysis.
[b]The degree of succinyl substitution of NSOC determined by elemental analysis.
[c]The degree of succinyl substitution of NSOC determined by ^{1}H-NMR.

The SEM images of CS and NSOC in Fig. 4 show a clear change in the surface morphology. It showed that CS presented a typically smooth and nonporous surface. On the contrary, the SEM image of NSOC showed the existence of many open loose pores on the surface, and such structures with loose pores were beneficial for mass transfer during Pb(II) adsorption onto the NSOC [29].

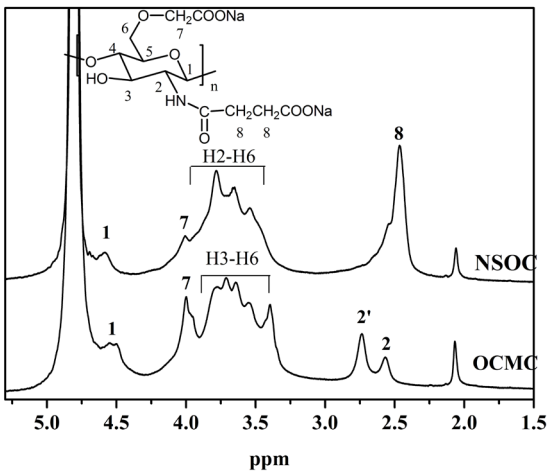

Fig. 3. ^{1}H-NMR spectra of OCMC and NSOC with D_2O as solvent.

Fig. 5 shows the XRD patterns for CS and NSOC. The broad peak of CS at 2θ = 20° indicated its partial crystalline nature [30]. However, the intensity of the characteristic peak at 2θ = 20° of NSOC decreased more than that of CS, and the crystalline peak was almost disappeared. It is well known that the XRD peak is related to the size of crystallite; the weaker peak usually results from small crystallites [15]. It was thought that the decrease in crystallinity of NSOC could be attributed to the deformation of the strong hydrogen bond in the CS backbone chain, as the hydroxyl and amino groups had been substituted [31].

3.2. Effect of pH on adsorption

The pH value of the adsorption medium is an important factor influencing adsorption of heavy metal ions onto adsorbent. In this study, the effects of initial pH values on the adsorption of Pb(II) onto CS and NSOC were studied at a pH value range of 2.0–5.5. This pH range was chosen because Pb(II) get precipitated above pH 5.5. The results are depicted in Fig. 6(a). As indicated in Fig. 6, the adsorption capacities of

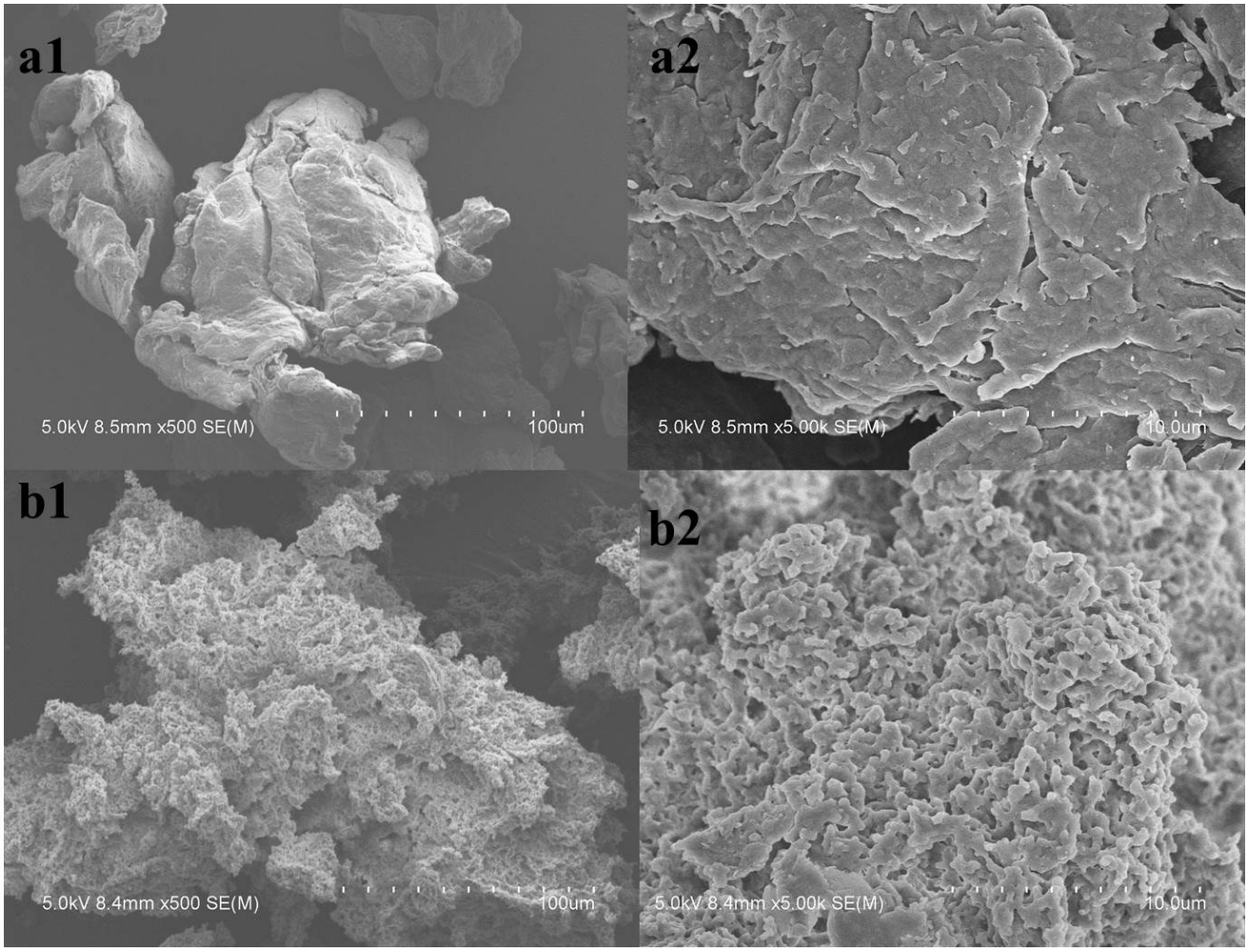

Fig. 4. SEM photographs: (a1) CS sample 500×; (a2) CS sample 5,000×; (b1) NSOC sample 500×; and (b2) NSOC sample 5,000×.

Pb(II) on CS and NSOC both increased sharply with increasing pH of Pb(II) solution from 2.0 to 3.0 and then increased gradually with further increasing pH to 5.5. The maximum adsorption capacities of Pb(II) was 66.8 and 368.4 mg/g for CS and NSOC at pH 5.5, respectively.

The main mechanisms influencing the adsorption characteristics can be explained by ion exchange, chelation and electrostatic attraction. Primary amino and carboxyl groups

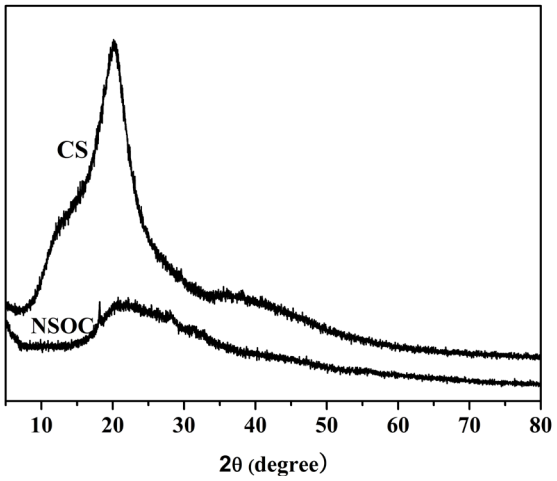

Fig. 5. XRD patterns of CS and NSOC.

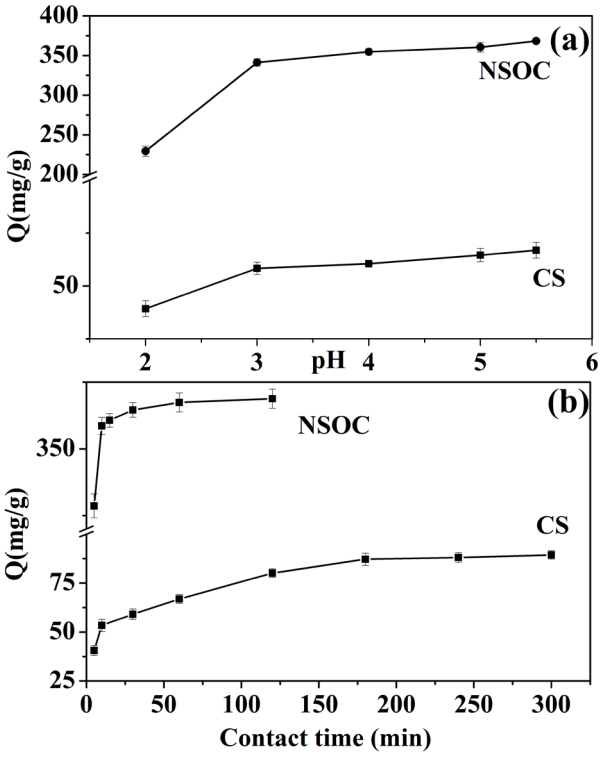

Fig. 6. (a) Effect of pH on adsorption of Pb(II) by CS and NSOC ([Pb(II)]: 1,000 mg/L; adsorbent dose: 100 mg/50 mL; *T*: 25°C; contact time: 60 min) and (b) effect of contact time on adsorption of Pb(II) by CS and NSOC ([Pb(II)]: 1,000 mg/L; adsorbent dose: 100 mg/50 mL; *T*: 25°C; pH 5.5 for Pb(II)).

are highly reactive with heavy metals, because nitrogen atom of amino group and oxygen atom of carboxyl group hold free electron doublets and can react with heavy metal ions [32]. At acid conditions, most of the amino groups of CS were protonated and converted into $–NH_3^+$. The electrostatic repulsion between Pb(II) and $–NH_3^+$ could also prevent the adsorption of Pb(II). With the increase of pH value, the concentration of H^+ ions decreased and facilitated the adsorption of metal ions via electrostatic interaction [33].

A similar pattern was observed for Pb(II) ions on NSOC. At a lower pH values, most of $–COO^–$ groups in NSOC adsorbent were changed to –COOH; therefore, the adsorption was attributed to ion exchange between Pb(II) and –COOH. Moreover, an excess of H^+ could compete effectively with Pb(II) for binding sites, resulting in a lower metal uptake capacity. As the pH of solution increased, some –COOH groups turned into $–COO^–$ groups, which would attract positively charged metal ions due to chelation or electrostatic attraction.

3.3. Adsorption kinetics

The adsorption rate related with the contact time (*t*) is one of the important characteristics that define the efficiency of adsorption, and it is usually described by adsorption kinetics. The effects of contact time on the adsorption of CS and NSOC for Pb(II) are shown in Fig. 6(b). It can be seen that Pb(II) adsorption on NSOC was a very fast process comparing with CS. The amounts of adsorption of Pb(II) increased rapidly in the first 10 min, contributing to 97.2% of the ultimate adsorption capacity, and then increased slowly and approached the adsorption equilibrium in about 120 min, with an equilibrium uptake of 368.8 mg/g in this case. However, the adsorption capacities of Pb(II) on CS increased to 53.4 mg/g in 10 min, contributing to 59.7% of the ultimate adsorption capacity, and then augmented slowly to an equilibrium uptake of 89.4 mg/g in 300 min. In a word, fast kinetics is characteristic in adsorption of Pb(II) on the NSOC and is desirable and beneficial for practical adsorption applications in wastewater treatment because a higher adsorption capacities are reached in shorter times [34]. Furthermore, the Pb(II) adsorption capacity of NSOC was 4.13 times of that of CS. The spontaneously high rate of metal ion uptake and excellent adsorption capacity of NSOC were associated with the significant number of carboxyl groups and high chemical reactivity of carboxyl groups for heavy metals.

In order to investigate the mechanism of adsorption, pseudo-first-order and pseudo-second-order models had been exploited to analyze the experimental data [35,36]. The equations of the two kinetic models are given as follows:

$$\log(Q_e - Q_t) = \log Q_e - \frac{k_1}{2.303}t \tag{5}$$

$$\frac{t}{Q_t} = \frac{1}{k_2 Q_e^2} + \frac{t}{Q_e} \tag{6}$$

where Q_e is the amount of metal ions adsorbed at equilibrium (mg/g); Q_t is the amounts of metal adsorbed at *t* time (mg/g); k_1 is the pseudo-first-order adsorption rate constant (min^{-1});

and k_2 is the constant of pseudo-second-order adsorption (g/min mg). The rate constant k_1 and correlation coefficients were determined by plotting the $\log(Q_e - Q_t)$ against t, and the straight-line plots of t/Q_t vs. t were used to calculate the rate constant k_2 and other kinetics parameters similarly. Table 2 shows the kinetic parameters of the two models, and the linearized form are shown in Fig. S1.

On the basis of the correlation coefficients (R^2) in Table 2, the adsorption behaviors of Pb(II) on CS and NSOC fitted well with the pseudo-second-order kinetic model compared with the pseudo-first-order model. The calculated Q_e values were in agreement with the theoretical ones, and the plots showed quite good linearity with R^2 above 0.99. Therefore, the adsorption kinetics follows the pseudo-second-order model, suggesting that chemisorption is the dominant rate-limiting step [37].

3.4. Adsorption isotherms

Adsorption isotherms are important for describing the adsorption mechanism for the interaction of heavy metals on the adsorbent surface. Two of the most commonly used isotherm theories have been adopted in this work, namely the Langmuir and Freundlich [38]. In this study, Both Langmuir and Freundlich models were used to study the adsorption equilibrium, and they can be represented by the following equations:

$$\frac{C_e}{Q_e} = \frac{C_e}{Q_m} + \frac{1}{K_L Q_m} \tag{7}$$

$$\ln Q_e = \frac{1}{n}\ln C_e + \ln K_F \tag{8}$$

where Q_e and C_e are the amounts adsorbed (mg/g) and the adsorbate concentration on solution (mg/L), respectively, both at equilibrium; K_L is the Langmuir isotherm constants indicating the affinity of adsorbent for metal ions; Q_m (mg/g) is the maximum adsorption capacity for monolayer formation on adsorbent. K_F is a unit capacity coefficient; and n is the Freundlich constant associated to the degree of system heterogeneity [39].

The adsorption of Pb(II) onto NSOC fitted to the Langmuir (plotting C_e/Q_e vs. C_e) and Freundlich (plotting $\ln Q_e$ vs. $\ln C_e$) isotherm models is shown in Fig. 7. It was found that the Langmuir model was much better to describe the adsorption of Pb(II) onto NSOC than the Freundlich model, indicating that the adsorption process was mainly monolayer adsorption. The parameters of Langmuir and Freundlich adsorption isotherms, evaluated from the linear plots, are presented in Table 3. It can been seen that the Q_{max} values (381.7 mg/g) for the adsorption of Pb(II) onto NSOC calculated from the Langmuir model were in close proximity to the experimental data. As a comparison, the isotherm adsorption data of Pb(II) on CS are also presented in Fig. 7. The Langmuir isotherm model also appeared to give an adequate fit to the experimental data, and the maximum adsorption capacity for Pb(II) was calculated to be 100.6 mg/g. Therefore, the grafting of carboxyl groups on CS significantly enhanced the adsorption capacity of the adsorbent.

The maximum adsorption capacities (Q_m) for Pb(II) adsorption onto other modified CS derivatives are compared in Table 4. It could be seen that the Q_m values varied considerably for different adsorbents and the NSOC adsorbent exhibits a good capacity to adsorb Pb(II) from aqueous solutions.

3.5. Adsorption mechanism of Pb(II) on NSOC

To understand the nature of adsorption and identify the possible sites of Pb(II) binding to NSOC, FTIR spectra were obtained for NSOC before and after Pb(II) adsorption in Fig. 2. After adsorption, the bands of asymmetric and symmetric stretching vibrations of carboxylic anions ($–COO^-$) in NSOC shifted obviously from 1,577 and 1,412 cm^{-1} to 1,562 and 1,406 cm^{-1}, respectively, which indicated that carboxyl groups were chelating functional groups for Pb(II) [44]. The characteristic band of stretching vibration of C–OH shifted slightly from 1,066 to 1,065 cm^{-1} after adsorption, suggesting that the oxygen atoms in the hydroxyl groups of NSOC were not involved in Pb(II) adsorption, at least not through complexation or other chemical mechanisms. Besides, the amide I band (NHCO) at 1,646 cm^{-1} was unchanged after adsorption, which indicated that NHCO groups were not participated in adsorption.

To verify the findings from the FTIR spectra, XPS analysis was used to determine the chemical states of the functional groups on the NSOC surface before and after Pb(II) adsorption. The C 1s, N 1s and O 1s XPS spectra are shown in Fig. 8, and the binding energy (BE) data of C 1s, O 1s and N 1s is summarized in Table 5. As shown in Fig. 8 and Table 5, C 1s XPS spectrum of NSOC showed three characteristics peaks corresponding to C–C and C–H bonds (285.08 eV), C–O bond (286.21 eV) and –COO bond (287.93 eV) [45]. The peak at 399.68 eV was contributed to the N in the –NHCO– group. Moreover, the XPS spectra of C 1s and N 1s did not show any noticeable change after Pb(II) adsorption, indicating that these atoms were not involved in the chemical adsorption of Pb(II).

There were two BE peaks in O 1s spectrum before adsorption of Pb(II) ions at 531.35 and 532.68 eV, which

Table 2
Kinetic parameters for the adsorption of Pb(II) on chitosan and NSOC

Adsorbent	$q_{e\text{-exp}}$ (mg/g)	Pseudo-first order			Pseudo-second order		
		$q_{e\text{-cal}}$ (mg/g)	k_1 (min^{-1})	R^2	$q_{e\text{-cal}}$ (mg/g)	k_2 (g/mg·min)	R^2
CS	89.4	49.8	0.01559	0.98	92.8	0.00079	0.99
NSOC	368.8	24.6	0.05117	0.85	370.4	0.00593	0.99

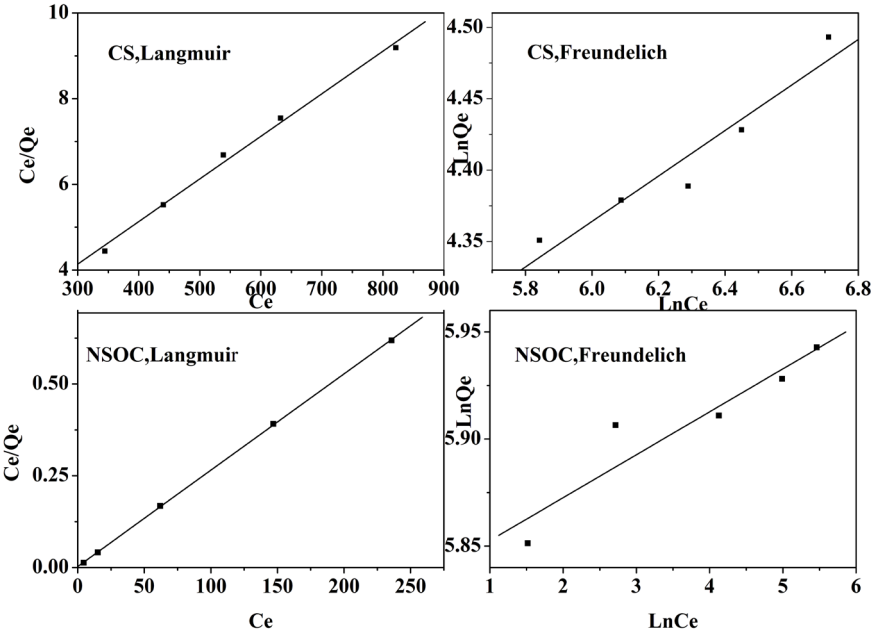

Fig. 7. Langmuir and Freundlich plots for the adsorption of Pb(II) onto CS and NSOC.

Table 3
Langmuir and Freundlich isotherm parameters for Pb(II) adsorption on chitosan and NSOC

	Langmuir			Freundlich		
	Q_m (mg/g)	K_L (L/mg)	R^2	K_F	n	R^2
CS	100.6	0.0086	0.99	30.21	6.28	0.93
NSOC	381.7	0.9066	0.99	341.22	49.9	0.88

Table 4
Comparison of maximum adsorption capacities of various adsorbents for Pb(II)

Type of adsorbent	Q_m (mg/g)	Reference
The poly(acrylic acid)-functionalized chitosan	294.1	[1]
Cross-linked *N*-succinyl chitosan resin with Pb(II) as template ions	329.4	[17]
N-carboxymethyl chitosan	421.9	[23]
Xanthate-modified magnetic chitosan	76.9	[40]
Ethylenediaminetetraacetic acid (EDTA)-modified cross-linked chitosan	265.2	[41]
Chitosan-coated zero valent iron nanoparticles	666.6	[42]
EDTA-cross-linked magnetic chitosan	213.4	[43]
NSOC	381.7	This work

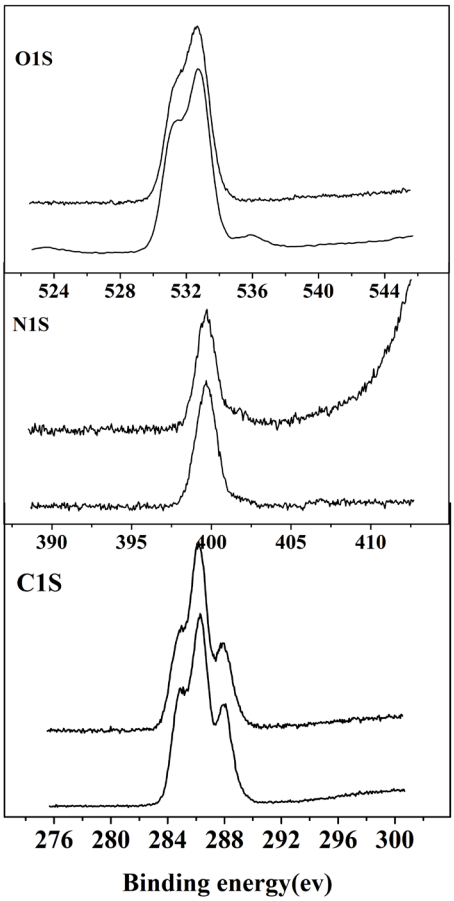

Fig. 8. The C 1s, N 1s and O 1s XPS spectra of NSOC before (bottom) and after (top) Pb(II) adsorption.

Table 5
BEs of C 1s, O 1s and N 1s on XPS spectra obtained by NSOC before and after Pb(II) adsorption

XPS data	C 1s	N 1s	O 1s
NSOC	285.08 (C–C), 286.21 (C–O), 287.93 (C=O)	399.68 (N–C=O)	531.35 (C=O), 532.68 (C–O)
NSOC-Pb(II)	285.00 (C–C), 286.13 (C–O), 287.83 (C=O)	399.73 (N–C=O)	531.68 (C=O), 532.68 (C–O)

were assigned to the oxygen atoms in the –COO groups and –C–OH, respectively [46]. After metal uptake, the peak of –COO shifted to higher BE from 531.35 to 531.68 eV while peak of C–O at 532.68 eV remained the same. This phenomenon can be attributed to the formation of O=C–O—Pb(II) complexes, in which a lone pair of electrons in the oxygen atom was donated to the shared bond between the O and Pb(II). On the other hand, the hydroxyl group was not involved in Pb(II) binding. In summary, on the basis of the results of XPS and FTIR analysis, a large number of carboxyl groups were the main adsorption sites in Pb(II) adsorption. Amide and hydroxyl groups were not involved in Pb(II) adsorption.

4. Conclusions

A novel NSOC chelating resin containing carboxyl and succinyl functional groups was obtained by a two-step method and well characterized by FTIR, elemental analysis, ^{1}H-NMR, SEM and XRD. The NSOC is highly efficient in removing Pb(II) ions from aqueous solution. The equilibrium adsorption of NSOC for Pb(II) reached 368.8 mg/g, 4.13 times higher than that of CS. The adsorption isotherms of Pb(II) on NSOC obey the Langmuir equation, and the kinetic data follow a pseudo-second-order model. FTIR and XPS spectra suggested that carboxyl groups of NSOC participated in the adsorption.

Acknowledgments

This work was supported by the National Natural Science Foundation of China (21405001, 51303002) and the Natural Science Foundation of Anhui Province (1508085MB27), which are gratefully acknowledged.

References

[1] N. Li, R.B. Bai, Highly enhanced adsorption of lead ions on chitosan granules functionalized with poly(acrylic acid), Ind. Eng. Chem. Res., 45 (2006) 7897–7904.
[2] W.S.W. Ngah, M.A.K.M. Hanafiah, Removal of heavy metal ions from wastewater by chemically modified plant wastes as adsorbents: a review, Bioresour. Technol., 99 (2008) 3935–3948.
[3] W.S.W. Ngah, L.C. Teong, M.A.K.M. Hanafiah, Adsorption of dyes and heavy metal ions by chitosan composites: a review, Carbohydr. Polym., 83 (2011) 1446–1456.
[4] E. Guibal, M. Van Vooren, B.A. Dempsey, J. Roussy, A review of the use of chitosan for the removal of particulate and dissolved contaminants, Sep. Sci. Technol., 41 (2006) 2487–2514.
[5] A. Demirbas, Heavy metal adsorption onto agro-based waste materials: a review, J. Hazard. Mater., 157 (2008) 220–229.
[6] M.A. Bhat, H. Chisti, S.A. Shah, Removal of heavy metal ions from water by cross-linked potato di-starch phosphate polymer, Sep. Sci. Technol., 50 (2015) 1741–1747.
[7] A.J. Varma, S.V. Deshpande, J.F. Kennedy, Metal complexation by chitosan and its derivatives: a review, Carbohydr. Polym., 55 (2004) 77–93.
[8] M.A. Kamal, T. Yasin, L. Reinert, L. Duclaux, Adsorptive removal of copper (II) ions from aqueous solution by silane cross-linked chitosan/PVA/TEOS beads: kinetics and isotherms, Desal. Wat. Treat., 57 (2016) 4037–4048.
[9] R. Yang, H.J. Li, M. Huang, H. Yang, A.M. Li, A review on chitosan-based flocculants and their applications in water treatment, Water Res., 95 (2016) 59–89.
[10] Q.P. Song, C.X. Wang, Z. Zhang, J.G. Gao, Adsorption of Cu(II) and Ni(II) using a novel xanthated carboxymethyl chitosan, Sep. Sci. Technol., 49 (2014) 1235–1243.
[11] L. Xu, J. Chen, Y.Z. Wen, H. Li, J.Q. Ma, D.M. Fu, Fast and effective removal of cadmium ion from water using chitosan encapsulated magnetic Fe_3O_4 nanoparticles, Desal. Wat. Treat., 57 (2016) 8540–8548.
[12] V. Balan, L. Verestiuc, Strategies to improve chitosan hemocompatibility: a review, Eur. Polym. J., 53 (2014) 171–188.
[13] F.P. Zhao, E. Repo, D.L. Yin, M.E. Sillanpää, Adsorption of Cd(II) and Pb(II) by a novel EGTA-modified chitosan material: kinetics and isotherms, J. Colloid Interface Sci., 409 (2013) 174–182.
[14] R. Jayakumar, M. Prabaharan, S.V. Nair, S. Tokura, H. Tamura, N. Selvamurugan, Novel carboxymethyl derivatives of chitin and chitosan materials and their biomedical applications, Prog. Mater. Sci., 55 (2010) 675–709.
[15] Q.P. Song, Z. Zhang, J.G. Gang, C.M. Ding, Synthesis and property studies of *N*-carboxymethyl chitosan, J. Appl. Polym. Sci., 119 (2011) 3282–3285.
[16] S.L. Sun, Q. Wang, A.Q. Wang, Adsorption properties of Cu(II) ions onto *N*-succinyl-chitosan and crosslinked *N*-succinyl-chitosan template resin, Biochem. Eng. J., 36 (2007) 131–138.
[17] S.L. Sun, A.Q. Wang, Adsorption properties of *N*-succinyl-chitosan and cross-linked *N*-succinyl-chitosan resin with Pb(II) as template ions, Sep. Purif. Technol., 51 (2006) 409–415.
[18] W.Y. Xiong, Y. Yi, H.Z. Liu, H. Wang, J.H. Liu, G.Q. Ying, Selective carboxypropionylation of chitosan: synthesis, characterization, blood compatibility, and degradation, Carbohydr. Res., 346 (2011) 1217–1223.
[19] X.G. Chen, H.J. Park, Chemical characteristics of *O*-carboxymethyl chitosans related to the preparation conditions, Carbohydr. Polym., 53 (2003) 355–359.
[20] F.L. Mi, S.J. Wu, Y.C. Chen, Combination of carboxymethyl chitosan-coated magnetic nanoparticles and chitosan-citrate complex gel beads as a novel magnetic adsorbent, Carbohydr. Polym., 131 (2015) 255–263.
[21] N. Flores-Alamo, R.M. Gómez-Espinosa, M. Solache-Ríos, J.L. García-Rivas, R.E. Zavala-Arce, B. García-Gaitán, Adsorption behaviour of copper onto a novel modified chitosan material: thermodynamic study, Desal. Wat. Treat., 57 (2016) 25080–25088.
[22] L. Wang, Q. Li, A.Q. Wang, Adsorption of cationic dye on *N*,*O*-carboxymethyl-chitosan from aqueous solutions: equilibrium, kinetics, and adsorption mechanism, Polym. Bull., 65 (2010) 961–975.
[23] C.X. Wang, Q.P. Song, J.G. Gao, Investigation of adsorption capacity of *N*-carboxymethyl chitosan for Pb(II) ions, Water Sci. Technol., 68 (2013) 1873–1879.
[24] G.Z. Kyzas, P.I. Siafaka, E.G. Pavlidou, K.J. Chrissafis, D.N. Bikiaris, Synthesis and adsorption application of succinyl-grafted chitosan for the simultaneous removal of zinc and cationic dye from binary hazardous mixtures, Chem. Eng. J., 259 (2015) 438–448.
[25] H.T. Pang, X.G. Chen, H.J. Park, D.S. Cha, J.F. Kennedy, Preparation and rheological properties of deoxycholate-chitosan and carboxymethyl-chitosan in aqueous systems, Carbohydr. Polym., 69 (2007) 419–425.
[26] H. Zheng, X.Q. Zhang, F.L. Xiong, Z.J. Zhu, B. Lu, Y.H. Yin, P.H. Xu, Y.M. Du, Preparation, characterization, and tissue distribution in mice of lactosaminated carboxymethyl chitosan nanoparticles, Carbohydr. Polym., 83 (2011) 1139–1145.

[27] Z.T. Lin, K. Song, J.P. Bin, Y.L. Liao, G.B. Jiang, Characterization of polymer micelles with hemocompatibility based on *N*-succinyl-chitosan grafting with long chain hydrophobic groups and loading aspirin, J. Mater. Chem., 21 (2011) 19153–19165.
[28] A.P. Zhu, T. Chen, L.H. Yuan, H. Wu, P. Lu, Synthesis and characterization of *N*-succinyl-chitosan and its self-assembly of nanospheres, Carbohydr. Polym., 66 (2006) 274–279.
[29] G.L. Huang, H.Y. Zhang, J.X. Shi, T.A.G. Langrish, Adsorption of chromium(VI) from aqueous solutions using cross-linked magnetic chitosan beads, Ind. Eng. Chem. Res., 48 (2009) 2646–2651.
[30] S.K. Mishra, S. Kannan, Development, mechanical evaluation and surface characteristics of chitosan/polyvinyl alcohol based polymer composite coatings on titanium metal, J. Mech. Behav. Biomed. Mater., 40 (2014) 314–324.
[31] H.C. Ge, Z.W. Ma, Microwave preparation of triethylenetetramine modified grapheneoxide/chitosan composite for adsorption of Cr(VI), Carbohydr. Polym., 131 (2015) 280–287.
[32] S. Zhang, Y.F. Zhou, W.Y. Nie, L.Y. Song, T. Zhang, Preparation of uniform magnetic chitosan microcapsules and their application in adsorbing copper ion(II) and chromium ion(III), Ind. Eng. Chem. Res., 51 (2012) 14099–14106.
[33] J.P. Zhang, A.Q. Wang, Adsorption of Pb(II) from aqueous solution by chitosan-*g*-poly(acrylic acid)/attapulgite/sodium humate composite hydrogels, J. Chem. Eng. Data, 55 (2010) 2379–2384.
[34] G.L. Dotto, M.L.G. Vieira, L.A.A. Pinto, Kinetics and mechanism of tartrazine adsorption onto chitin and chitosan, Ind. Eng. Chem. Res., 51 (2012) 6862–6868.
[35] T. Anitha, P.S. Kumar, K.S. Kumar, K. Sriram, J.F. Ahmed, Biosorption of lead(II) ions onto nano-sized chitosan particle blended polyvinyl alcohol (PVA): adsorption isotherms, kinetics and equilibrium studies, Desal. Wat. Treat., 57 (2016) 13711–13721.
[36] F.P. Zhao, E. Repo, D.L. Yin, Y. Meng, S. Jafari, M. Sillanpää, EDTA-cross-linked β-cyclodextrin: an environmentally friendly bifunctional adsorbent for simultaneous adsorption of metals and cationic dyes, Environ. Sci. Technol., 49 (2015) 10570–10580.
[37] W.S.W. Ngah, L.C. Teong, R.H. Toh, M.A.K.M. Hanafiah, Comparative study on adsorption and desorption of Cu(II) ions by three types of chitosan–zeolite composites, Chem. Eng. J., 223 (2013) 231–238.
[38] V. Dhanapal, K. Subramanian, Modified chitosan for the collection of reactive blue 4, arsenic and mercury from aqueous media, Carbohydr. Polym., 117 (2015) 123–132.
[39] F.P. Zhao, E. Repo, Y. Meng, X.T. Wang, D.L. Yin, M. Sillanpää, An EDTA-β-cyclodextrin material for the adsorption of rare earth elements and its application in preconcentration of rare earth elements in seawater, J. Colloid Interface Sci., 465 (2016) 215–224.
[40] Y.H. Zhu, J. Hu, J.L. Wang, Competitive adsorption of Pb(II), Cu(II) and Zn(II) onto xanthate-modified magnetic chitosan, J. Hazard. Mater., 221 (2012) 155–161.
[41] H.C. Ge, S.Y. Huang, Microwave preparation and adsorption properties of EDTA-modified cross-linked chitosan, J. Appl. Polym. Sci., 115 (2010) 514–519.
[42] M. Suguna, N.S. Kumar, V. Sreenivasulu, A. Krishnaiah, Removal of Pb(II) from aqueous solutions by using chitosan coated zero valent iron nanoparticles, Sep. Sci. Technol., 49 (2014) 1613–1622.
[43] F.P. Zhao, E. Repo, M. Sillanpää, Y. Meng, D.L. Yin, W.Z. Tang, Green synthesis of magnetic EDTA- and/or DTPA-cross-linked chitosan adsorbents for highly efficient removal of metals, Ind. Eng. Chem. Res., 54 (2015) 1271–1281.
[44] C.X. Wang, Q.P. Song, Removal of Cu(II) ions from aqueous solutions using *N*-carboxymethyl chitosan, Water Sci. Technol., 66 (2012) 2027–2032.
[45] L. Yue, L. Zhang, H. Zhong, Carboxymethyl chitosan: a new water soluble binder for Si anode of Li-ion batteries, J. Power Sources, 247 (2014) 327–331.
[46] H. Yan, J. Dai, Z. Yang, H. Yang, R.S. Cheng, Enhanced and selective adsorption of copper(II) ions on surface carboxymethylated chitosan hydrogel beads, Chem. Eng. J., 174 (2011) 586–594.

Supplementary information

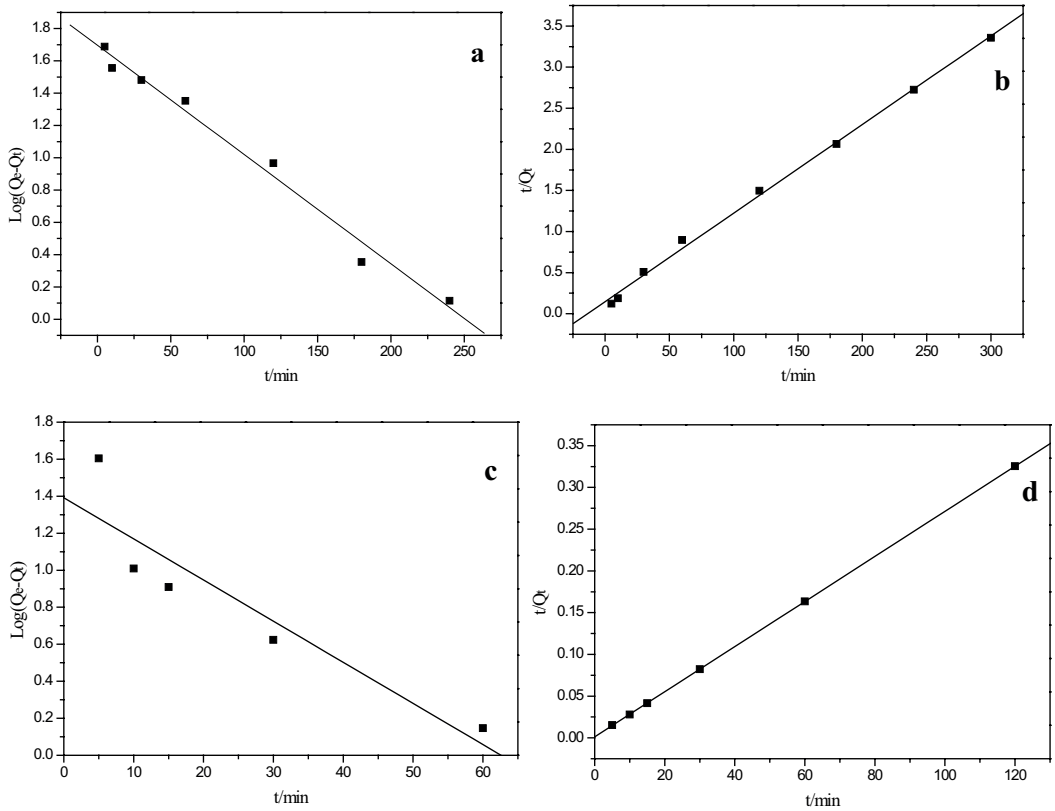

Fig. S1. Adsorption kinetics model fitted for: (a) pseudo-first-order model of Pb(II) adsorbed on chitosan; (b) pseudo-second-order model of Pb(II) adsorbed on chitosan; (c) pseudo-first-order model of Pb(II) adsorbed on NSOC and (d) pseudo-second-order model of Pb(II) adsorbed on NSOC.